Journal of Power Sources 238 (2013) 173–179

Contents lists available at SciVerse ScienceDirect

Journal of Power Sources

journal homepage: www.elsevier.com/locate/jpowsour

Novel synthesis and electrochemical performance of nano-structured composite with Cu_2O embedment in porous carbon as anode material for lithium ion batteries

Xueyang Shen, Shi Chen, Daobin Mu*, Borong Wu, Feng Wu

Beijing Key Laboratory of Environmental Science and Engineering, School of Chemical Engineering and Environment, Beijing Institute of Technology, Beijing 100081, China

HIGHLIGHTS

- A study on Cu_2O/porous carbon (PC) composite as a high performance anode for lithium ion batteries.
- The embedded structure of nano-sized Cu_2O in PC is helpful to the outstanding cycle stability.
- PC is capable of accommodating the large volume expansion of Cu_2O during cycles.
- The composite exhibits excellent reversible capacity and rate performance.

GRAPHICAL ABSTRACT

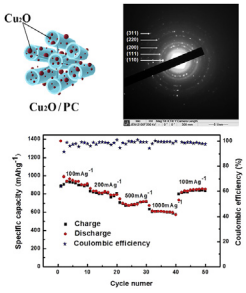

ARTICLE INFO

Article history:
Received 18 January 2013
Received in revised form
4 March 2013
Accepted 7 March 2013
Available online 26 March 2013

Keywords:
Cuprous oxide
Porous carbon
Anode material
Lithium ion batteries

ABSTRACT

The paper reports a novel nano-structured Cu_2O/porous carbon (PC) composite and its application as an anode material for lithium ion batteries. The architecture and the electrochemical performance of the as-prepared composite are investigated through structure characterization and galvanostatic charge/discharge test. Cu_2O nanoparticles are well-distributed in the pore channels owing to the nanoscale confinement effect apart from the edges of PC matrix. The composite exhibits a high reversible capacity of 884.4 mA h g^{-1} after 100 cycles, especially an excellent rate capability of 600.8 mA h g^{-1} when cycled at the current density of 1000 mA g^{-1}. The outstanding lithium storage properties may be attributed to the designed embedment structure of the composite. The nano-sized Cu_2O loaded in the PC promotes the reaction of lithiation/delithiation owing to the large contact area and short lithium ion diffusion distance. Additionally, PC with highly-developed porous structure is capable of accommodating large volume expansion of Cu_2O and preventing the aggregation of particles upon continuous cycling.

1. Introduction

In order to deal with the increasing pressure of energy depletion and environmental pollution, a clean, sustainable and efficient energy supply is essential for social and environmental development [1,2]. Among various renewable energies, lithium ion batteries (LIBs) are considered to be one of the most promising candidates owing to their outstanding merits. However, with the miniaturization and the multifunction of energy-consuming instruments, in particular the demand of power source in electric vehicles, higher capacity and rate performance are required for advanced LIBs [3,4]. As a key factor of LIBs, new anode materials are constantly being proposed including Si-based anode materials, metal (Sn, Al, Sb, etc.) and their alloys, transition metal oxides (Fe_2O_3, TiO_2, Co_2O_3, etc.) and conducting polymers [5–11], with a desire for higher lithium storage capacities than that of conventional graphite (372 mA h g^{-1}).

* Corresponding author. Tel.: +86 10 68918770; fax: +86 10 68918828.
E-mail address: mudb@bit.edu.cn (D. Mu).

0378-7753/$ – see front matter © 2013 Elsevier B.V. All rights reserved.
http://dx.doi.org/10.1016/j.jpowsour.2013.03.085

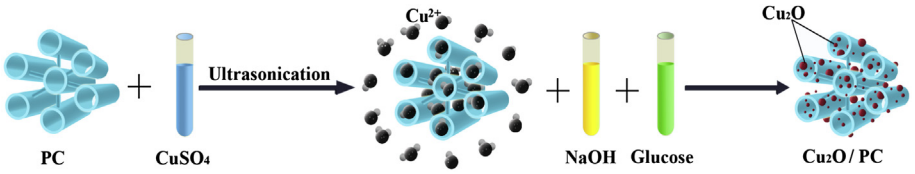

Fig. 1. Schematic illustration of the formation process of Cu_2O/PC composite.

For the attractive advantages such as the morphological diversity, facile synthesis and environmentally friendly, cuprous oxide (Cu_2O) has received much attention as a potential substitute for the LIBs anode [12,13]. Recently, a series of works have been involved in the study of Cu_2O-based anodes. Cu_2O materials with variant morphologies including nanotubes, hollow spheres, ordered porous film, starfish-like and cubic nanoparticles have been studied [14–18]. Hasan et al. also prepared core-shell Cu_2O/Cu composites through an electrode position technique, and attained a good capacity retention (about 450 mA h g^{-1}) at a high current density of 5 mA cm^{-2} [19]. Zhang et al. reported a green synthesis of Cu_2O–graphene hierarchical nanohybrids. Through the protection of graphene nanosheets, the as-obtained anode material exhibited an enhanced reversible specific capacity of over 400 mA h g^{-1} at a rate of 100 mA g^{-1} [20]. However, some problems have still to be concentrated on this Cu_2O anode like large irreversible capacity, unsatisfactory rate performance and specific capacity. The poor electrode stability caused by the volume changes of Cu_2O with lithiation/delithiation is not substantially solved yet. There is plenty of room for the improvement of the anode material in lithium storage performance.

Porous carbon (PC) materials have been paid more attention on the modification of anode materials because of their characteristics: abundant pore structures, large surface area and good electrical conductivity [21,22]. As a kind of typical PC, ordered CMK-3 was applied as the matrix of some metal oxides (CoO_x, SnO_2, TiO_2, etc.), which partly enhance the cycling behavior and the rate performance of composite electrodes [23–25]. However, its small pore size (~3–4 nm) would make it difficult to load the active materials inside the pores. Instead, it was reported that the Fe_3O_4/C composite showed high specific capacity and durable cycling performance using mesocellular carbon foams in pore size (>20 nm) as a host material [26]. Basically, appropriate pore size of the carbon matrix and suitable synthesis process are crucial for the subsequent loading of active materials, which will eventually have impact on the electrochemical performance.

Herein, we first unveil a nano-structured Cu_2O-based composite synthesized utilizing the porous carbon (PC) in big mesopore size to present a high lithium storage performance. PC with pore size ranging from 30 to 50 nm was designed to complete the composite fabrication in consideration with its large space to embed the active materials sufficiently. Through an ultrasound-assisted solution synthesis process, nano-sized Cu_2O is expected to grow on the channels of PC owing to the nanoscale confinement effect. Additionally, the porous structure will be beneficial for the touch of the electrolyte and provide the room to accommodate the large volume expansion of Cu_2O during lithiation/delithiation. The architecture and the electrochemical performances of Cu_2O/PC composite as an anode for LIBs are investigated in detail.

2. Experimental

2.1. Preparation of Cu_2O/PC composite

Porous carbon was prepared by a template method based on our previous work [27]. Gelatin and nano-$CaCO_3$ particulates (in size around 30–50 nm) were used as carbon source and template, respectively, (gelatin:$CaCO_3$ = 2:1, wt%). The calcination treatment was conducted at 700 °C for 2 h under argon atmosphere.

An ultrasound-assisted one-step solution method was applied to synthesize Cu_2O/PC composite, the schematic illustration of the formation process is described in Fig. 1. $CuSO_4 \cdot 5H_2O$ (1 g, 99 wt%) was dissolved in 15 mL of deionized water to form a blue homogeneous solution, then 0.8 g PC was added into the solution under magnetic stirring for 30 min. The above mixture was ultrasonic-processed continuously for 15 min before 12 mL of NaOH solution (0. 018 mol) and 16 mL of glucose solution (3.6 mmol) were added into it simultaneously. During intensive stirring at 70 °C for 25 min, the blue color of the solution gradually changed to dark brown, black and finally brick-red as the oxidation and the subsequent reduction proceeded. The brick-red precipitates were washed with deionized water and vacuum-dried at 50 °C for 10 h. Similarly, pure Cu_2O power was also prepared through the above one-step ultrasound-assisted solution method except the procedure of adding PC.

2.2. Characterization of Cu_2O/PC composite

The X-ray diffraction (XRD) measurements were taken on an Ultima IV diffractometer using Cu Kα radiation with a scan rate of 8° min^{-1} from 10° to 90°. The surface morphology was observed by

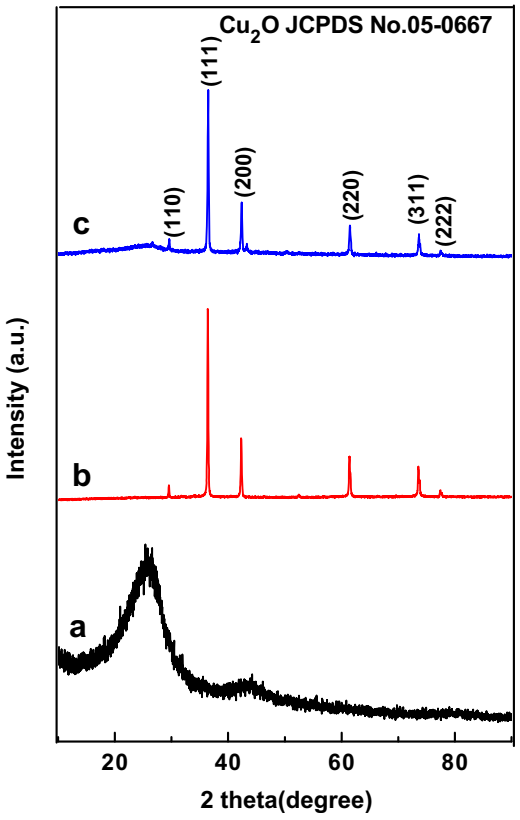

Fig. 2. XRD patterns of (a) PC, (b) Cu_2O and (c) Cu_2O/PC composite.

scanning electron microscopy (SEM, JEOL JSM-5600LV) and transmission electron microscopy (TEM, JEM-2100). Nitrogen adsorption/desorption isotherms were measured at 77 K on a NOVA1200 instrument (Quantachrome Corporation). The samples were degassed in a vacuum at 200 °C for 12 h prior to the measurement. The total specific area was determined by the multipoint Brunauer–Emmett–Teller method. The content of Cu_2O in the composite was evaluated by TG analysis at a temperature range of 30–800 °C with a heating rate of 10 °C min^{-1} under air atmosphere.

Electrochemical performance of the composite electrode was tested using coin-type cells (CR2025) assembled in an argon-filled glove box. The working electrode was prepared by pasting slurries onto a Cu foil, and dried at 100 °C for 10 h before testing. The slurry was made by mixing composite material, carbon black (Super P) and polyvinylidene fluoride (PVDF) in a weight ratio of 6:2:2. Lithium sheet acted as the counter electrode, 1 mol L^{-1} $LiPF_6$/EC + DEC solution as the electrolyte (EC:DEC = 1:1 in weight ratio) and Celgard 2300 film as the separator in the coin cell. Charge/discharge tests were carried out at a current density of 100 mA g^{-1} and a voltage range of 0.01–3 V employing a LAND2001 CT battery tester. Cyclic voltammetry (CV) of the electrode was measured at scan rates of 0.1, 0.2, 0.5 and 1 mV s^{-1}. Electrochemical impedance spectra were measured on fresh cells at open circuit voltage. Both the measurements of CV and impedance were conducted using a CHI 600D electrochemical analyzer. The voltages mentioned in this study were referred to Li/Li^+ redox couple.

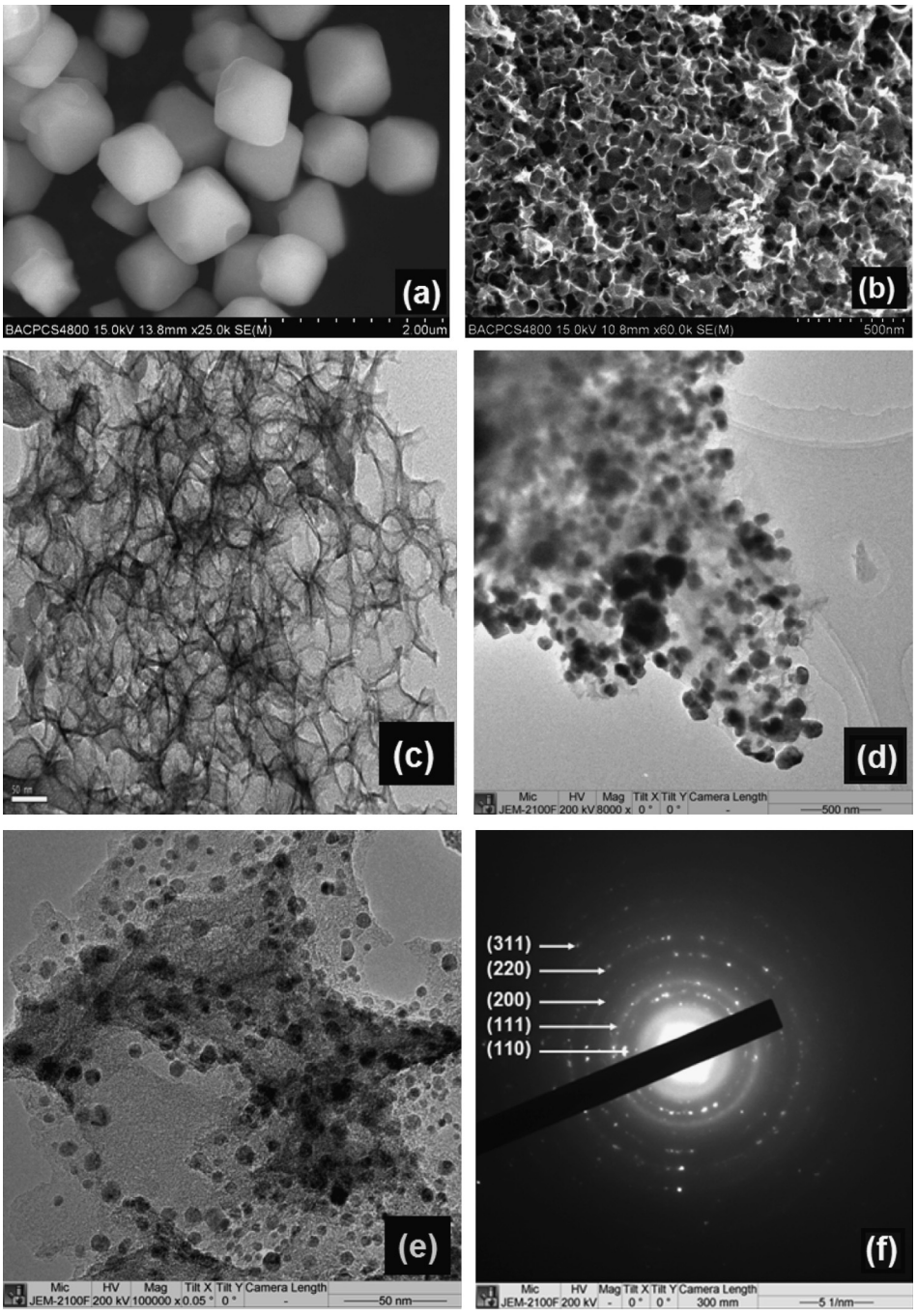

Fig. 3. SEM images of (a) Cu_2O and (b) PC, TEM images of (c) PC, (d) and (e) Cu_2O/PC composite, (f) selected area electron diffraction (SAED) pattern of Cu_2O/PC composite.

3. Results and discussion

X-ray diffraction (XRD) patterns of PC, Cu_2O and Cu_2O/PC composite are shown in Fig. 2. Two broad diffraction peaks at $2\theta = 23^\circ$ and 43° (Fig. 2(a)) can be indexed as the (002) and (100) planes of carbon, implying a non-graphitized carbon structure [28]. In Fig. 2(b) and (c), both of the XRD patterns show the diffraction peaks of Cu_2O at $2\theta = 29.7^\circ$, 36.7°, 42.7°, 61.6°, 73.5° and 77.3°, corresponding to the lattice plane of (110), (111), (200), (220), (311) and (222), respectively. The narrow and sharp peaks suggest highly crystalline nature of the obtained Cu_2O phase. In the pattern of Cu_2O/PC, besides the characteristic peaks ascribed to the Cu_2O, the broad diffraction peak at $2\theta = 23^\circ$ related to the non-graphitized carbon can also be seen clearly, indicating the existence of both Cu_2O and carbon phase in the as-prepared composite.

The SEM morphology of the Cu_2O crystals is shown in Fig. 3(a). It is found that the Cu_2O particles are uniform octahedra-shaped with an average diagonal distance about 1 μm. Such octahedra particles with no evident bulky aggregates are closely related to the growth environments and conditions in experiment. The honeycomb-like structure of PC with abundant porous fabrication is observed in Fig. 3(b). The carbon has a well-distributed pore size (30–50 nm) of nano-channels, exhibiting larger mesopores compared to CMK-3 synthetized by traditional silica template method [24,25]. So, it is possible to provide more appropriate space for the subsequent loading of Cu_2O particles. To gain further insight into the composite microstructure, the TEM image (Fig. 3(c)) of PC shows a turbostratic graphite structure, which is consistent with the XRD results. The low magnification image of Cu_2O/PC composite shown in Fig. 3(d) manifests the uniform distribution of Cu_2O within the PC matrix. It is apparent that the Cu_2O particles are limited to nanoscale (about 40 nm) compared to those synthesized separately, which is in favor of their embedment in the pores of the PC. From the higher magnification image in Fig. 3(e), it can be seen that the Cu_2O particles with smaller size (about 5 nm) are even well-distributed on the edges of PC. These phenomena can be explained as follows: Cu^{2+} migrates to inside the pores and the edges of PC by the ultrasonic treatment. The subsequent reduction of Cu^{2+} to Cu^{+} is limited because of the nanoscale confinement effect, leading directly to the reduced size of Cu_2O particle. Additionally, the rich active sites existed in the edges of PC facilitated the nanocrystallization of Cu_2O as well. In general, the porous structure of PC together with the synthesis method is conducive to the uniform distribution of Cu_2O in the carbon matrix. Selected area electron diffraction (SAED) pattern in Fig. 3(f) shows that all the diffraction rings can be indexed to the Cu_2O lattice structure, further indicating the composite comprises of Cu_2O phase with fine crystallinity.

The nitrogen adsorption/desorption isotherms are shown in Fig. 4(a). Both of the PC and Cu_2O/PC samples exhibit a typical type IV N_2 adsorption/desorption isotherm according to the IUPAC classification, having a typical H1 hysteresis loop in mesopore range and a sharp capillary condensation step at very high relative pressures ($p/p_0 > 0.9$). The PC sample shows a high specific surface area of 532.23 $m^2\ g^{-1}$ with a pore volume of 0.6426 $cm^3\ g^{-1}$. After the loading of Cu_2O, the specific surface area and pore volume of the Cu_2O/PC composite are reduced to 67.02 $m^2\ g^{-1}$ and 0.2362 $cm^3\ g^{-1}$, respectively. Evidently, it can be concluded that Cu_2O particles are embedded in the PC matrix through the in situ process of synthesis. Fig. 4(b) indicates that the pore size of PC primarily distributes in the range of 30–50 nm, which accords well with the observation of SEM image. Additionally, compared with the dV/d(log D) of PC, an obvious decrease of the value in the composite can be observed. These results demonstrate that the embedment structure of Cu_2O particles in the channels of PC is attained.

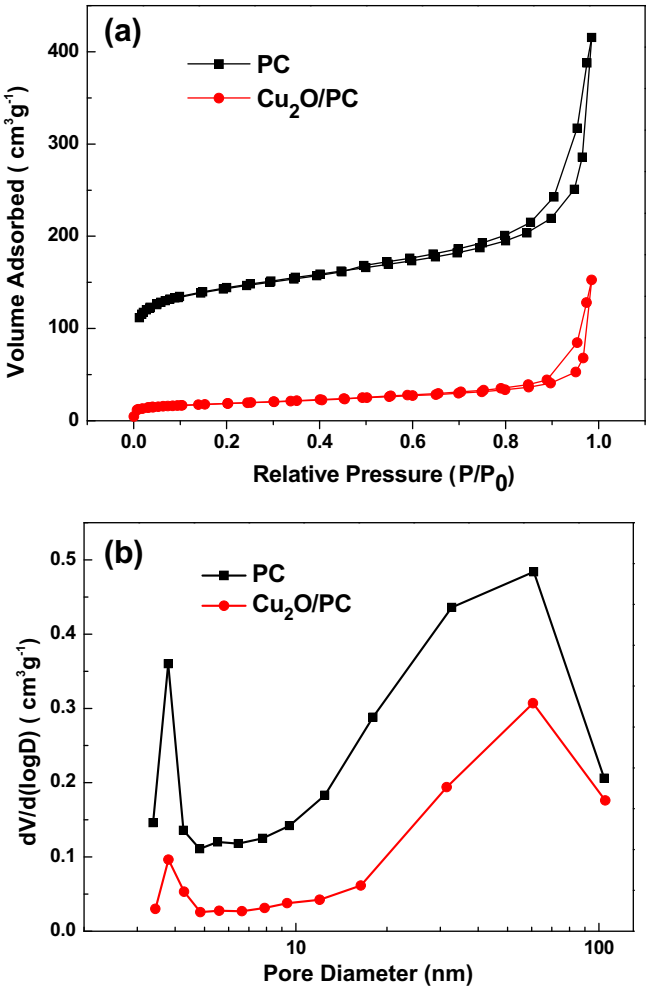

Fig. 4. (a) N_2 adsorption/desorption isotherms of PC and Cu_2O/PC composite, (b) pore size distributions of PC and Cu_2O/PC composite (the samples were degassed under vacuum at 200 °C for 12 h before the measurements).

In order to evaluate the Cu_2O content in the composite, thermogravimetric (TG) curves of the as-prepared Cu_2O and Cu_2O/PC composites are analyzed, as shown in Fig. 5. As for Cu_2O, a weight increase of 5% is found owing to the oxidation of Cu_2O with heat

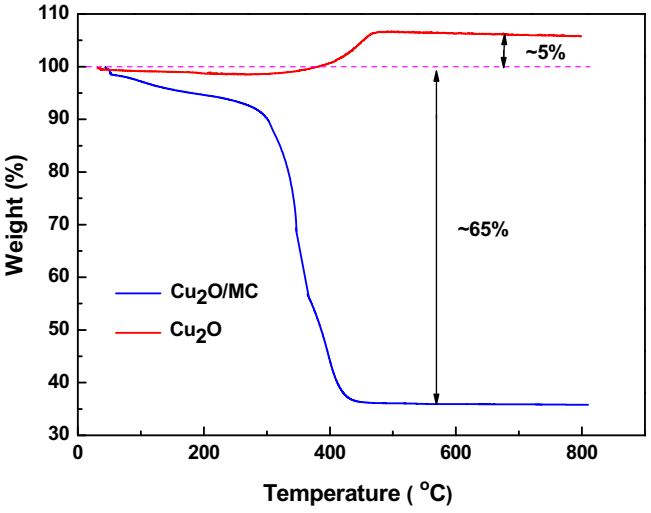

Fig. 5. TG curves of Cu_2O and Cu_2O/PC composite under air atmosphere from 30 °C to 800 °C.

treatment. Besides, there is a weight decrease (around 2%) from 100 °C to 250 °C which can be ascribed to the removal of water in the product. Thus the experimental mass increased for Cu_2O should be 7–8%. In the case of Cu_2O/PC composite, the removal of carbon leads to a weight loss of about 65% from 280 °C to 410 °C. Thus, in consideration of the joint contributions from these two aspects, the Cu_2O content is estimated approximately as 28 wt% in the composite.

Fig. 6(a), (c) and (e) shows the galvanostatic discharge/charge curves of Cu_2O, PC and Cu_2O/PC composite electrodes cycled at a current density of 100 mA g^{-1} over a voltage range of 0.01–3 V. In the first cycle, Cu_2O electrode exhibits discharge/charge (lithiation/delithiation) capacities of 538.3 mA h g^{-1} and 242 mA h g^{-1}, respectively, corresponding to a coulombic efficiency of 45%. A long discharge plateau at 1.2 V can be observed and disappears in subsequent cycles, which is thought to be the inducement of the initial irreversible capacity. As a comparison, the initial reversible capacity and coulombic efficiency of the as-prepared PC are 576.7 mA h g^{-1} and 50% (Fig. 6(c)), respectively. The long plateau near 0.2 V in discharge curve makes major contribution to the reversible capacity of the PC electrode. As for the Cu_2O/PC composite electrode, much higher discharge/charge capacities of 1383.9 mA h g^{-1} and 882.6 mA h g^{-1} are achieved in the first cycle, together with a coulombic efficiency of 64%. The improved initial coulombic efficiency can be ascribed to the loading of Cu_2O which decreases the surface area and the pore volume of PC. It is helpful to avoid the irreversible insertion of lithium ion via pore channels. The initial discharge curve shows two plateaus near 1.2 V and 0.2 V, meaning that the increased discharge capacity results from the contributions of both Cu_2O and PC.

Cyclic voltammograms of Cu_2O, PC and Cu_2O/PC composite electrodes are examined as shown in Fig. 6(b), (d) and (f). In the first cathodic half-cycle (lithiation) of pure Cu_2O and the composite electrode, there are strong reduction peaks appearing nearby 1.2 V in both cases, which should be assigned to the lithiation of Cu_2O. According to the "conversion reactions" mechanism of transition metal oxide [13,29], at the range of 1.2–1 V, Cu_2O reacts with the

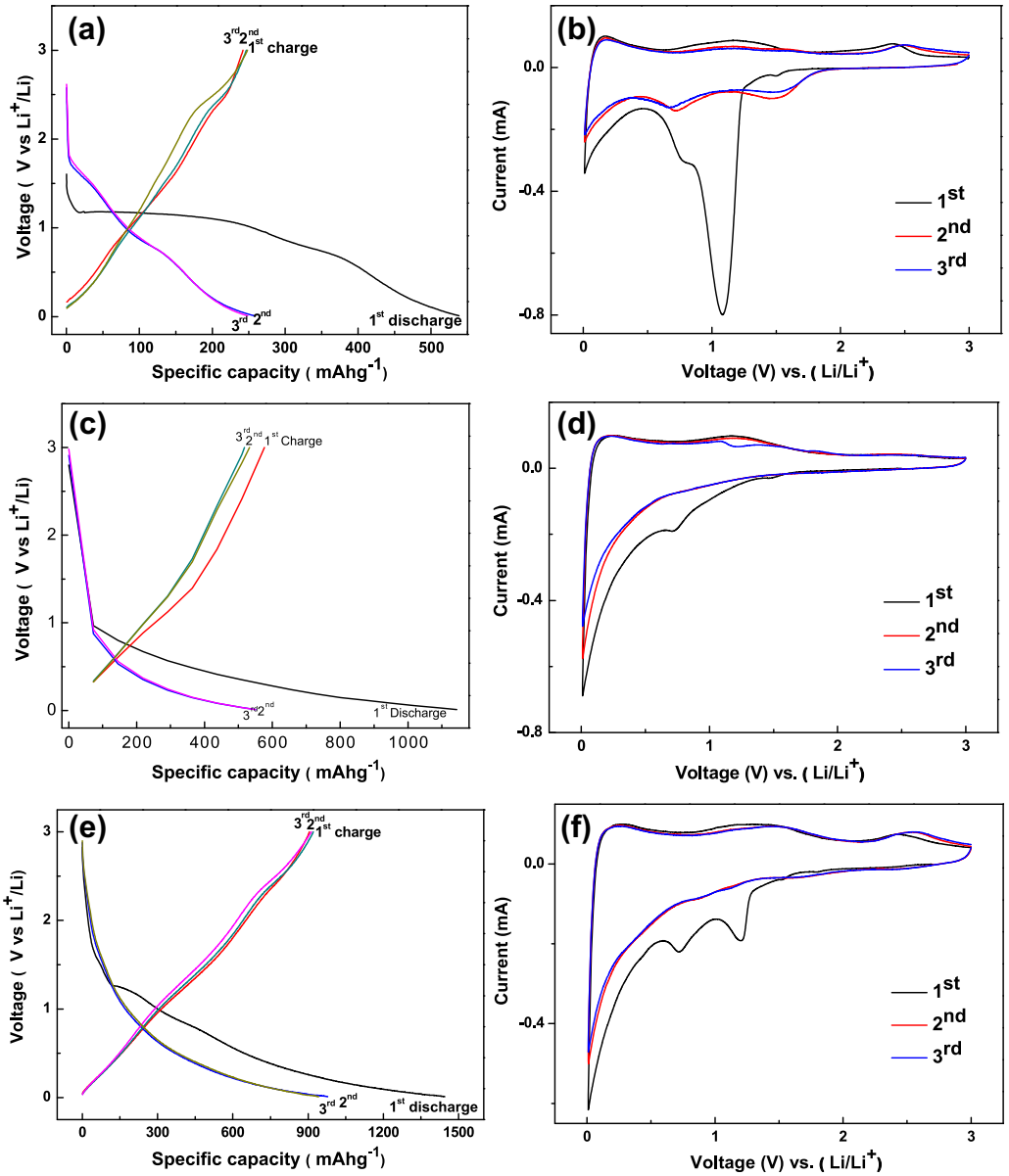

Fig. 6. Charge/discharge curves of (a) Cu_2O, (c) PC and (e) Cu_2O/PC composite electrode cycled between 0 and 3 V at a current density of 100 mA g^{-1}; Cyclic voltammogram curves of (b) Cu_2O, (d) PC and (f) Cu_2O/PC composite electrode in initial three cycles, the scan rate is 0.1 mV s^{-1}.

lithium ion and accepted two electrons before the formation of Cu and Li_2O. Besides, the weak reduction peak near 0.6 V is attributed to the formation of solid electrolyte interface (SEI) layer between Cu_2O and electrolyte [14], resulting in the initial irreversible capacity. In the anodic half-cycle (delithiation), an oxidation peak at about 2.4 V is ascribed to the re-formation of Cu_2O. Another oxidation peak at about 1.4 V is supposed to be caused by the decomposition of the SEI layer [30]. The results are coincident with the corresponding profiles of discharge/charge curves.

The cycling performance of the Cu_2O/PC, Cu_2O and PC electrodes at a current density of 100 mA g^{-1} is shown in Fig. 7. It is found that the Cu_2O/PC composite holds a high discharge capacity of 884.4 mA h g^{-1} after 100 cycles, which is far higher than the value of 435.2 mA h g^{-1} for PC materials at the same experimental condition. The Cu_2O electrode can only maintain a reversible capacity of 174 mA h g^{-1} in the 100th cycle. The reason for the remarkable improvement in the cyclic stability of the composite is that, firstly, PC with highly-developed porous structure is capable of accommodating large volume expansion of Cu_2O and preventing the aggregation of particles upon continuous cycling. Secondly, the nano-sized Cu_2O loaded in the PC promotes the reaction of lithiation/delithiation, which can be attributed to the large contact area and short lithium ion diffusion distance of nanoscale materials [13,31]. In contrast, the larger size of the as-prepared pure Cu_2O particle has a negative impact on its electrochemical properties. Furthermore, as a result of the strong adsorption characteristics of PC, the pulverization of Cu_2O during cycles can be effectively avoided since the lithiation/delithiation reactions can be constrained in channels. In a word, the designed embedment structure of the composite is beneficial to the outstanding cycle stability and reversibility.

The rate performance of Cu_2O/PC composite is investigated as shown in Fig. 8(a). The reversible capacities of the composite maintain 897, 792.2 and 719.2 mA h g^{-1} at the current rates of 100, 200 and 500 mA g^{-1}, respectively. In particular, a high capacity of 600.8 mA h g^{-1} can still be obtained when cycled at 1000 mA g^{-1}. The composite also keeps steady coulombic efficiency (>98%) along with the increasing current densities. It is indicates that a stable solid electrolyte interface (SEI) film is formed, ensuring the reversibility of the electrochemical reactions in the subsequent cycles [32]. As shown in Fig. 8(b), CV curves at different scan rates were examined to discuss the rate performance. It can be seen that even at a high scan rate of 1 mV s^{-1}, the positions of the oxidation peaks have no apparent shift, implying the good reversibility. In case of the reduction processes, the peaks shift slightly with the

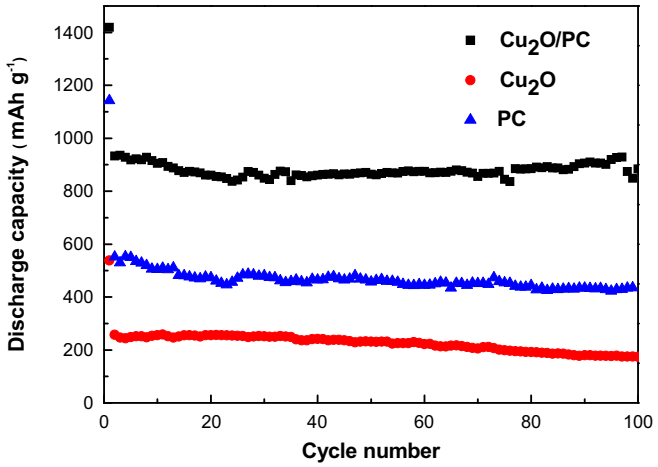

Fig. 7. Cycling performance of Cu_2O/PC composite, Cu_2O and PC at a current density of 100 mA g^{-1}.

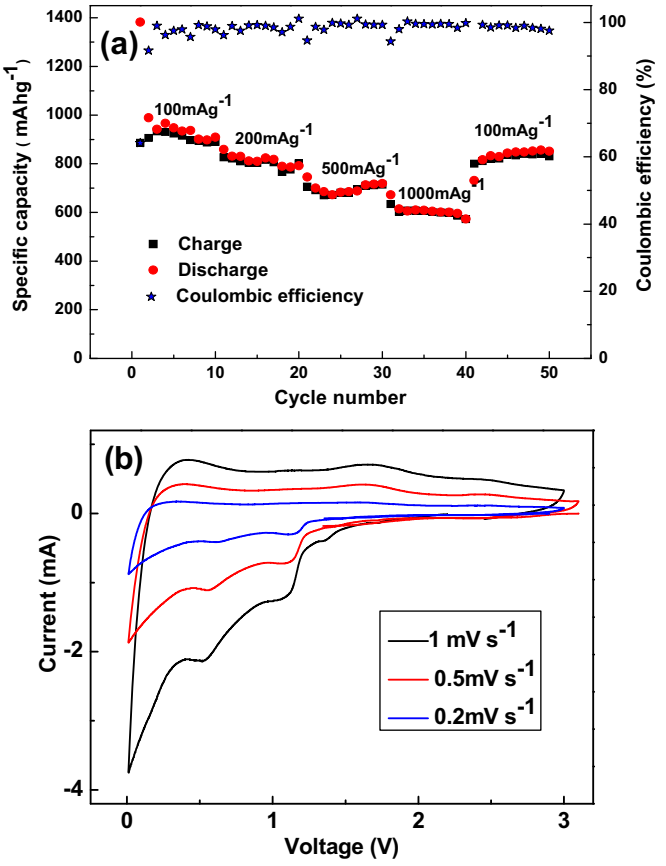

Fig. 8. (a) Rate performance of Cu_2O/PC composite cycled between 0.1 and 3V, (b) cyclic voltammetry curves of Cu_2O/PC composite at the scan rate of 0.2, 0.5 and 1 mV s^{-1}, respectively.

increase of scan rate, inevitably leading to the decreased capacity, which is reflected in the rate performance with increasing currents. The superior rate capability may be attributed to the electrochemical reactivity of nano-sized Cu_2O loaded in the PC matrix. Moreover, PC network with an excellent conductivity provides a conducting medium among Cu_2O nanoparticles to modify the electrical contact of the composite, thereby enhancing its rate capability.

Fig. 9(a) presents the electrochemical impedance spectra (EIS) on Cu_2O and Cu_2O/PC electrodes. The Nyquist plots of the electrodes contain one semicircle in the high frequency region and an inclined line in the low frequency region. The electron transfer resistance (R_{ct}) value of the Cu_2O/PC composite electrode is estimated as 61.4 Ω, which is much lower than that of pure Cu_2O electrodes (594.9 Ω). Obviously, the reactivity of the composite is greatly improved owing to the synergistic effect of PC and active Cu_2O nanoparticles loaded in the matrix. The diffusion coefficient of lithium ion can be calculated according to the equation [33]:

$$D_{Li^+} = \frac{R^2T^2}{2A^2F^4C^2n^4\sigma^2} \quad (1)$$

where R is the gas constant, T is the absolute temperature, A is the surface area of the electrode, F is the Faraday constant, C is the concentration of Li^+ in the electrode, n is the number of reacting electron, σ is Warburg factor following the relationship:

$$Z_{re} = \sigma \cdot \omega^{-1/2} \quad (2)$$

In terms of the linear relationship between Z_{re} and $\omega^{-1/2}$ in Fig. 9(b), σ is obtained from the slope of the line. It is 34.9 for the

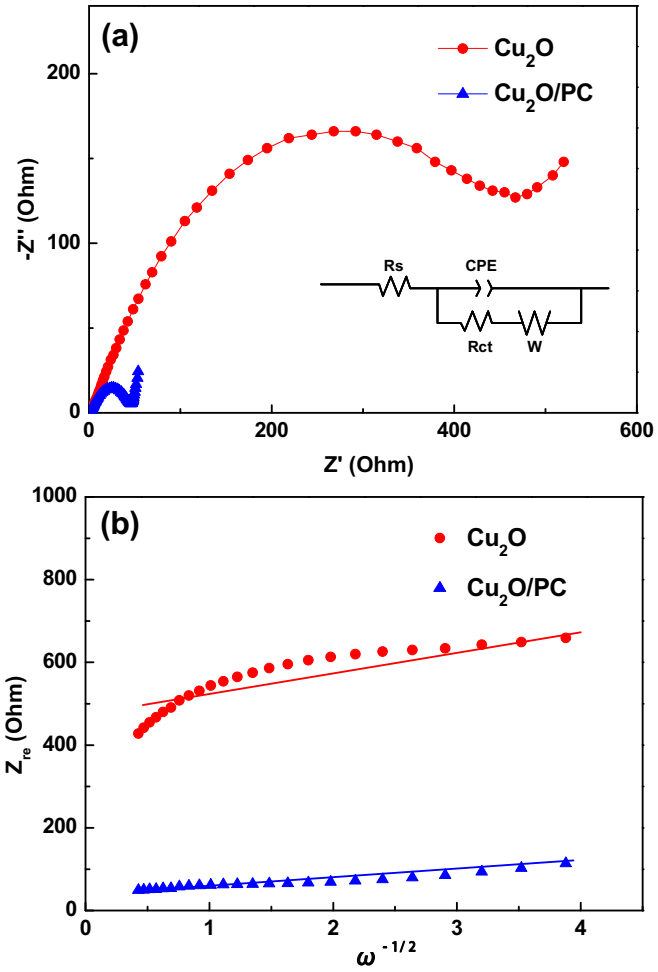

Fig. 9. (a) Nyquist plots at the OCP and the equivalent circuit for Cu_2O/PC composite and pure Cu_2O electrodes. (b) The relationship between Z_{re} and $\omega^{-1/2}$ for Cu_2O/PC composite and pure Cu_2O electrodes.

Cu_2O/PC composite and 268.5 for pure Cu_2O. By combining the above two equations, the lithium diffusion coefficient of Cu_2O/PC material is calculated as 4.12×10^{-13} cm^2 s^{-1}, while the value is 1.99×10^{-17} cm^2 s^{-1} for pure Cu_2O. The result confirms that lithium ion migration is also promoted in the composite besides the electron transfer.

4. Conclusions

In this paper, we design and synthesize a novel Cu_2O/PC composite as LIBs anode materials. Nano-sized Cu_2O particles are relatively well-distributed in the pore channels and edges of the PC matrix. The as-prepared Cu_2O/PC composite displays an excellent reversible capacity of 884.4 mA h g^{-1} at a current density of 100 mA g^{-1} after 100 cycles, together with a high rate capacity of 600.8 mA h g^{-1} cycled at 1000 mA g^{-1}. The improved lithium storage properties can be attributed to the synergistic effect between nano-sized embedded Cu_2O and PC matrix. PC is capable of accommodating large volume expansion and preventing the aggregation of Cu_2O upon continuous discharge/charge cycling. Besides, the porous nanostructure of the composite can also promote the migration of lithium ion and facilitate electrolyte infiltration, resulting in the outstanding high rate capacity and large reversible capacity.

Acknowledgment

We acknowledge the National 973 Program (Grant No. 2009CB220100) and the National 863 Program (2013AA050903) of China for the financial support to the work. We also thank the support from U.S.–China Clean Energy Research Center Clean Vehicles Consortium (Grant No. 2010DFA72760-101).

References

[1] J.B. Goodenough, Acc. Chem. Res. (2012), http://dx.doi.org/10.1021/ar2002705.
[2] V. Subramanian, H.W. Zhu, B.Q. Wei, J. Phys. Chem. B 110 (2006) 7178.
[3] S. Chandrashekar, N.M. Trease, H.J. Chang, L.S. Du, C.P. Grey, A. Jerschow, Nat. Mater. 11 (2012) 311.
[4] R. Teki, M.K. Datta, R. Krishnan, T.C. Paker, P.N. Kumta, N. Koratkar, Small 5 (2009) 2236.
[5] X.J. Feng, J. Yang, P.F. Gao, J.L. Wang, Y.N. Nuli, RSC Adv. 2 (2012) 5701.
[6] J.I. Lee, N.S. Choi, S. Park, Energy Environ. Sci. 5 (2012) 7878.
[7] J. Chen, X.H. Xia, J.P. Tu, Q.Q. Xiong, Y.X. Yu, X.L. Wang, C.D. Gu, J. Mater. Chem. 22 (2012) 15056.
[8] C. Lai, H.Z. Zhang, G.R. Li, X.P. Gao, J. Power Sources 196 (2011) 4735.
[9] H. Xiong, H. Yildirim, E.V. Shevchenko, V.B. Prakapenka, B. Koo, M.D. Slater, M. Balasubramanian, S. Sankaranarayanan, J.P. Greeley, S. Tepavcevic, N.M. Dimitrijevic, P. Podsiadlo, C.S. Johnson, T. Rajh, J. Phys. Chem. C 116 (2012) 3181.
[10] B. Sun, J. Horvat, H.S. Kim, W.S. Kim, J. Ahn, G.X. Wang, J. Phys. Chem. C 114 (2010) 18753.
[11] G.A. Snook, P. Kao, A.S. Best, J. Power Sources 196 (2011) 1.
[12] H.G. Yu, J.G. Yu, S.W. Liu, S. Mann, Chem. Mater. 19 (2007) 4327.
[13] P. Poizot, S. Laruelle, S. Grugeon, L. Dupont, J.M. Tarascon, Nature 407 (2000) 496.
[14] W.J. Liu, G.H. Chen, G.H. He, W. Zhang, J. Nanopart Res. 13 (2011) 2705.
[15] C.Q. Zhang, J.P. Tu, X.H. Huang, Y.F. Yuan, X.T. Chen, F. Mao, J. Alloys Compd. 441 (2007) 52.
[16] B.X. Li, X.F. Wang, D.D. Xia, Q.X. Chu, X.Y. Liu, F.G. Lu, X.D. Zhao, J. Solid State Chem. 184 (2011) 2097.
[17] J.C. Park, J. Kim, H. Kwon, H. Song, Adv. Mater. 21 (2009) 803.
[18] A. Lamberti, M. Destrob, S. Biancoa, M. Quaglioa, A. Chiodoni, C.F. Pirri, C. Gerbaldi, Electrochim. Acta 70 (2012) 62.
[19] M. Hasan, T. Chowdhury, J. Rohan, ECS Trans. 27 (2009) 3.
[20] Y. Zhang, X. Wang, L. Zeng, S.Y. Songb, D.P. Liu, Dalton Trans. 41 (2012) 4316.
[21] M. Yang, Q. Gao, Microporous Mesoporous Mater. 143 (2011) 230.
[22] Y. Mao, H. Duan, B. Xu, L. Zhang, Y.S. Hu, C.C. Zhao, Z.X. Wang, L.Q. Chen, Y.S. Yang, Energy Environ. Sci. 5 (2012) 7950.
[23] H.J. Liu, H.H. Bo, W.J. Cui, F. Li, C.X. Wang, Y.Y. Xia, Electrochim. Acta 53 (2008) 6497.
[24] G.L. Xu, S.R. Chen, J.T. Li, F.S. Ke, L. Huang, S.G. Sun, J. Electroanal. Chem. 656 (2010) 185.
[25] Y. Ishii, Y. Kanamori, T. Kawashita, I. Mukhopadhyay, S. Kawasaki, J. Phys. Chem. Solids 71 (2010) 511.
[26] E. Kang, Y.S. Jung, A.S. Cavanagh, G. Kim, S.M. George, A.C. Dillon, J.K. Kim, J. Lee, Adv. Funct. Mater. 21 (2011) 2430.
[27] X.Y. Shen, D.B. Mu, S. Chen, B. Xu, B.R. Wu, F. Wu, J. Alloys Compd. 552 (2013) 60.
[28] H.S. Zhou, S.M. Zhu, M. Hibi, I. Honma, M. Ichihara, Adv. Mater. 15 (2003) 2107.
[29] L.C. Yang, L.L. Liu, Y.S. Zhu, X.J. Wang, Y.P. Wu, J. Mater. Chem. 22 (2012) 13148.
[30] L.J. Fu, J. Gao, T. Zhang, Q. Cao, L.C. Yang, Y.P. Wu, R. Holze, H.Q. Wu, J. Power Sources 174 (2007) 1197.
[31] Y.H. Lee, I.C. Leu, S.T. Chang, C.L. Liao, K.Z. Fung, Electrochim. Acta 50 (2004) 553.
[32] L.X. Zeng, F.Y. Xiao, J.C. Wang, S.K. Gao, X.K. Ding, M.D. Wei, J. Mater. Chem. 10 (2012) 1039.
[33] X.Y. Wang, H. Hao, J.L. Liu, T. Huang, A.S. Yu, Electrochim. Acta 56 (2011) 4065.